Appl. Phys. A 64, 341–351 (1997)

Applied Physics A Materials Science & Processing

© Springer-Verlag 1997

Invited paper

Near-field photocurrent spectroscopy: A novel technique for studying defects and aging in high-power semiconductor lasers

Ch. Lienau, A. Richter, J.W. Tomm

Max-Born-Institut für Nichtlineare Optik und Kurzzeitspektroskopie, Rudower Chaussee 6, D-12489 Berlin, Germany
(Fax: +49-30/6392-1476, E-mail: lienau@mbi-berlin.de)

Received: 28 October 1996/Accepted: 5 November 1996

Abstract. We present the first comparative study of spatially resolved near-field photocurrent spectra for high power laser diode arrays with different wave guide characteristics before and after accelerated aging of the laser device. Sub-wavelength spatial resolution is demonstrated by using a near-field fiber probe as the excitation source. The potential of the technique for analyzing microscopic aging processes in optoelectronic devices is demonstrated. The experiments provide insight into mechanisms of defect formation within the p-i-n junction of InAlGaAs/GaAs laser diodes upon aging. The effect of the wave guide structure and of surface recombination processes on the near-field photocurrent images is discussed and analyzed in terms of a beam propagation model. The non-destructiveness makes this technique a particularly attractive method for *in-situ* analysis in high power laser diodes.

PACS: 07.60.Pb; 42.55.Px; 85.30.Fg; 85.60.Jb

With the increasing growth of the solid state laser market, the role of high power laser diode arrays becomes more and more important. Diode arrays are used for a number of applications, such as pumping of solid state lasers, the generation of blue and UV radiation by frequency doubling and material processing purposes. The high power density in these devices and the high light intensity near their mirror facets causes changes in the structure of the active laser material which ultimately limit the lifetime of the device. Consequently, a microscopic understanding of aging processes of high-power laser diodes is of utmost importance for increasing the performance and the lifetime of these devices. This problem has been addressed by a variety of techniques and reviews on this subject have been given by Fukuda [1] and Eliseev [2]. Moreover, from a more fundamental point of view, high power lasers present unique model systems for studying processes of defect creation and migration initiated by the high internal electrical field.

An understanding of aging mechanisms in current diode laser arrays is complicated, compared to single emitter diodes, by the fact that the properties of the device may vary strongly from emitter to emitter. This is demonstrated in Fig. 1, which shows a spatially resolved photocurrent signal (with a resolution of 30 μm) of a 50 element InAlGaAs laser array for below band gap excitation at 940 nm before and after 24 hours of operation. The non-aged laser diode shows no significant spatial variation of the photocurrent signal between adjacent emitters which are separated by 200 μm. In contrast, the PC signal of the aged diode fluctuates strongly from emitter to emitter. In particular, two of the 50 emitters of the array, show an strongly increased photocurrent signal which is more than two times larger than that of the other emitters.

Such observations make the quest for microscopic analysis techniques pertinent. Most recently, Near-Field Photocurrent Spectroscopy (NPCS) has been introduced by our group as a new analytical tool for monitoring microscopic aging processes in high-power laser diodes [3]. In this technique [4–6] the near-field radiation transmitted through a nanometer-sized

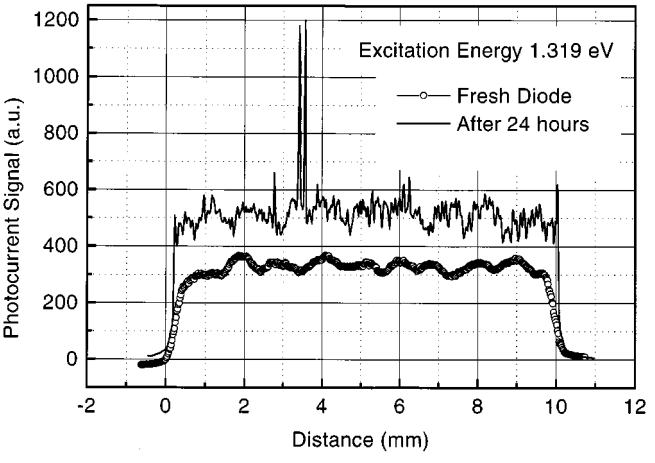

Fig. 1. Macroscopic photocurrent line scans at an excitation energy of 1.319 eV (940 nm) of a DQW step index laser diode array consisting of fifty 60 μm wide emitters separated by 140 μm before and after accelerated aging. While the fresh laser diode shows no significant variation of the photocurrent signal across the diode array, the signal of the aged diode fluctuates strongly from emitter to emitter. In particular, two of the 50 emitters of the array, located at about 3.5 mm, show a photocurrent signal which is more than two times larger than that of the other emitters. The spatial resolution in these experiments was about 30 μm

aperture is used to generate photocarriers which induce a photocurrent inside the sample acting basically as a photodiode. If the aperture is placed in close proximity to the sample, the excitation spot size is determined by the sub-wavelength size of the aperture and can thus be reduced to below 50 nm. The resolution of the NPCS experiment is determined by the excitation spot size, the absorption length of the radiation and minority carrier transport processes and could be shown to be better than 250 nm [4]. The technique presents several features that make it particularly attractive for the analysis of laser diodes. It combines high spatial resolution with non-destructiveness and the possibility of resonant excitation by using a tunable wavelength light source. This allows for the analysis of laser devices at different stages of aging without affecting the device performance by the analysis process.

In this paper, the technique is used for the first time to compare microscopic aging effects on high power laser diode structures with different wave guide characteristics. Aging effects on defect concentrations within the active layer and on (near-) surface radiationless recombination processes are resolved. The structure of the laser device is shown to play an important role for the image formation process, which is analyzed in terms of a ray tracing model.

The paper is outlined as follows. After a brief description of the experimental setup, we present macroscopic photocurrent spectra of the investigated structures. Then NPCS experiments obtained for a graded index diode array before and after accelerated aging are analyzed and discussed. These results are then compared to experiments performed on a step index array. Finally, the findings are summarized.

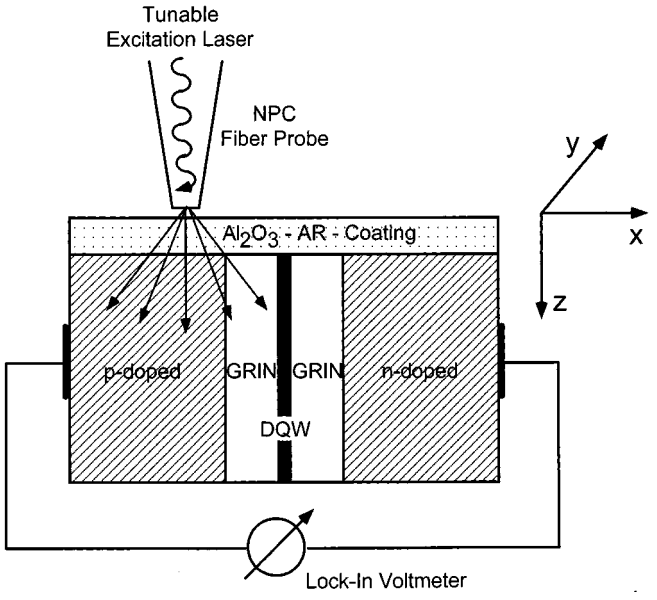

Fig. 2. Experimental setup of the near-field photocurrent (NPC) experiments. In these experiments, the laser diode is excited by tunable continuous-wave laser light transmitted through a nanometer-sized aperture located at the end of a near-field fiber probe. The near-field probe consists of a tapered single mode optical fiber with a lateral metal coating and aperture diameter between 50 and 200 nm. The photoinduced voltage (or current) across the p-i-n junction of the laser diode is detected as a function of the tip position as the laser diode, which is mounted on an *x-y-z* piezo, is scanned relative to probe tip. During the scan the tip to sample distance was kept constant at 5 ± 1 nm using an optical shear force setup. The photoinduced signal was detected with a lock-in nanovoltmeter with the laser diode unbiased. The layer structure of the DQW-GRIN laser diode array, consisting of two 12 nm GaAs quantum wells surrounded by 220 nm wide undoped $Al_{1-x}Ga_xAs$ ($0.3 < x < 0.6$) graded gap layers and by two, p- respectively n-doped 1.5–2 μm thick $Al_{0.6}Ga_{0.4}As$ cladding is shown schematically

1 Experimental

In the near-field photocurrent experiments, the laser diode is excited by light transmitted through a nanometer-sized aperture at the end of a NSOM probe tip [7]. The photoinduced voltage (or current) across the p-i-n junction of the laser diode is then detected as a function of the tip position as the laser diode, which is mounted on an *x-y-z* piezo, is scanned relative to probe tip (Fig. 2) [4, 5]. During the scan, the tip to sample distance was kept constant at 5 ± 1 nm by using a modified version of the optical shear force setup proposed by [8, 9]. The shear force mechanism relies on the damping of resonant lateral vibrations of the probe tip as the tip approaches the sample surface to within 10–20 nm. Such resonant lateral vibrations of the probe tip with amplitudes of less than 10 nm are excited with a dither piezo. The amplitude of the tip vibration is measured by focusing the output of a 670 nm laser diode onto the vibrating tip and imaging the resulting diffraction image onto a quadrant photodiode. The AC part of the photodiode signal provides a direct measure of the vibration amplitude and is fed into an electronic feedback system which controls the separation between the tip and the facet of the laser diode by adjusting the *z*-piezo voltage. Therefore, the *z*-piezo voltage gives direct information on the topography of the sample surface. Such shear-force images of the *z*-piezo voltage as a function of lateral tip position are recorded simultaneously with the near-field photocurrent images and provide a spatial correlation between the NPC signal and the layer structure of the laser diode.

The near-field optical microscope used for these experiments is based on a commercial instrument (Topometrix Aurora). Probe tips with a cone angle of 10° were pulled from single-mode optical fibers in a commercial CO_2-laser based fiber puller (Sutter) and then coated with a 50 to 100 nm thick aluminum or gold coating. The diameter of the uncoated tips was less than 30 nm as was demonstrated by scanning electron microscopy. Shear force images recorded with these uncoated tips gave a lateral resolution of better than 12 nm. The optical resolution of the aluminum or gold coated tips was tested using a standard AFM grating and was better than 50 nm. The piezoscanner was software linearized and calibrated against a standard AFM grating with a calibration error of less than ±5%. The scan range in these experiments was typically $10 \times 10\,\mu m^2$ and 100×100 or 200×200 data points were recorded for each scan. Tunable continuous wave laser sources (Cr:LiSAF, Ti:Sapphire) and a HeNe laser were used for excitation. The photoinduced voltage was collected with a lock-in nanovoltmeter at the n- and p-contacts of the unbiased laser diode. The excitation light was amplitude modulated at a frequency of 1 kHz. The power of the excitation light coupled into the fiber probe was about 3 mW and that of the light transmitted through the fiber probe varied between 10 and 100 nW, when detected in the far field. At these excitation powers, heating of the fiber tip [10] did not influence the NPCS experiments. The detected photoinduced voltage varied between 1 μV and 1 mV. Macroscopic

photocurrent spectra were recorded with a standard optical microscope giving a spatial resolution of 30 µm, a halogen lamp, a monochromator and a lock-in nanovoltmeter [11].

Two different high power InAlGaAs/GaAs laser diode array structures were investigated in this work. The layer sequence of both structures has been described earlier in more detail [12]. The first structure is a Double Quantum Well (DQW) Graded Index Separate Confinement Heterostructure (GRIN-SCH) grown by metalorganic vapor deposition on a n-type GaAs substrate. The DQW is situated in a symmetric valley formed by two 220 nm wide undoped $Al_{1-x}Ga_xAs$ ($0.3 < x < 0.6$) graded gap layers. These are surrounded by two, p- respectively n-doped 1.5–2 µm thick $Al_{0.6}Ga_{0.4}As$ cladding layers with an energy gap (E_g) of about 2.2 eV. The doping profile has its main gradient inside the DQW-GRIN-region. The second structure is a Step Index (SIN) DQW device, where the DQW region is embedded in an undoped 220 nm wide $Al_{0.3}Ga_{0.7}As$ layer ($E_g = 1.8$ eV). In both devices only the contact stripes provide gain guidance and thus form the array structure which was mounted p-side down on a copper heat sink. The front facet reflectivity was adjusted by a 120 nm thick Al_2O_3 layer to about 5%. The photon energy of the laser emission of all devices was determined to be $\hbar\omega = 1.53$ eV ($\lambda = 808$ nm). Accelerated aging was realized at 20 to 50 °C for up to 1200 h. The aging procedure and the changes of the device parameters are discussed in more detail elsewhere [11].

2 Results and discussion

2.1 Macroscopic photocurrent spectra

A macroscopic photocurrent (PC) spectrum (in arbitrary units, *full circles*) for a fresh DQW-GRIN laser diode emitting at a photon energy of 1.53 eV (808 nm) is depicted in Fig. 3a. The spectra was measured with a spatial resolution of 30 µm. The calculated spectral shapes of the absorption edge of the DQW $\alpha_{DQW}(\hbar\omega)$ and of the bottom of the GRIN structure $\alpha_{GRIN}(\hbar\omega)$ are added as solid and dotted lines (in cm^{-1}), respectively. In these experiments, the laser array serves as a photodiode driven by the incident light at a specific photon energy. The spectral shape of the PC spectrum is closely connected to the absorption coefficient of the entire structure. For all spectral positions, the PC signal magnitude correlates with the sum of the contributions $\sum\alpha_i(\hbar\omega)$ (see Fig. 3a) from the different layers (i). Furthermore it depends on the gradient of the sum potential consisting of contributions of the band edges and the doping profile, as well as on the diffusion of the photogenerated carriers into the intrinsic region and, as will be shown below, also on the penetration depth of the excitation light into the laser structure.

Three characteristic contributions to the PC spectrum are resolved. The most prominent feature is the strong signal increase at energies above 1.5 eV, i.e. above the effective band gap of the DQW structure of 1.53 eV. This evidently arises from the onset of the interband absorption of the transition from the first heavy hole to the first electron subband ($1\,hh \rightarrow 1\,e$) in the DQW (solid line in Fig. 3a). The reverse transition is responsible for the laser emission. In the energy range between 1.55 eV and 1.75 eV, the PC signal intensity remains roughly constant. At energies above 1.75 eV absorption

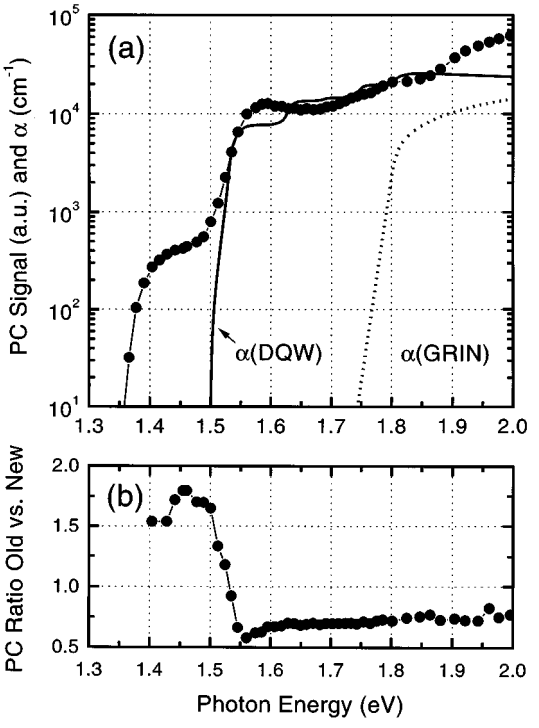

Fig. 3. a Macroscopic room-temperature photocurrent (PC) spectrum (*full circles*, in a.u.) of a fresh DQW-GRIN high power laser diode with an emission energy of 1.53 eV. Three characteristic features are resolved: (1) A weak below band gap shoulder at energies between 1.3 and 1.5 eV which is attributed to defect or impurity related absorption; (2) the DQW signal which dominates the spectrum at energies above 1.55 eV; and (3) absorption by the graded gap layers which gives rise to an increase of the PC signal at energies above 1.8 eV. The calculated absorption coefficients (cm^{-1}) of the DQW and the bottom of the GRIN region are depicted as a full and a dotted line, respectively; **b** Ratio of the macroscopic photocurrent signals after and before an accelerated aging test of the DQW-GRIN high power laser diode. Note the strong increase of the defect related below-band gap contribution, while the DQW signal of the aged diode at energies above 1.55 eV decreases only slightly

by the graded gap layers sets in (dotted line) and this causes another increase in signal intensity at higher energies.

The third feature in the PC spectrum is the weak broadband shoulder below the effective band edge (1.53 eV) which extends from energies of 1.5 eV to at least 1.35 eV. Fourier-Transform PC measurements carried out on these samples revealed that this shoulder extends even further into the infrared, at least down to 0.8 eV [13]. Such a below band gap contribution to the PC spectrum requires a low energy absorption mechanism such as, e.g., defect-band transitions. The energy dependence of the PC spectrum alone does not allow for an unequivocal assignment of the microscopic nature of these transitions. However, one can speculate, that aging of the diode laser enhances the creation and migration of native point defects such as vacancies. Such processes are likely to influence the PC spectra more strongly than, e.g. the migration of foreign atoms (such as the doping materials) into the active layer. The influence of native defects on the below band gap absorption is discussed in [14–16].

Based on the comparison of experimental absorption spectra of bulk GaAs and the calculated spectral dependence of the photoionization cross section of the deep donor EL2 level, Martin [14] concluded that the near-infrared optical absorption in undoped bulk GaAs is essentially due to the EL2 donor. This center is thought to be related to either isolated antisite

As_{Ga} defects or to complexes between arsenic atoms occupying a gallium site and surrounding vacancies [17]. Tüzemen and Brozels photoquenching experiments [15] discriminate between at least two native defects contributing to the optical absorption in the spectral region discussed here. With positron annihilation experiments in GaAs, Saarinen et al. [16] identified both Ga and As vacancies and suggested that the below band gap absorption is caused by optical transitions related to these vacancies. Thus it is very likely that there is a close correlation between laser aging and point defect creation or migration.

Upon accelerated aging of the laser device, the PC spectrum changes significantly, see Fig. 3b. The PC signal of the below band gap defect band **increases** by about 75% for energies below 1.5 eV. At energies above 1.55 eV, however, where the PC signal arises predominantly from the interband absorption of the 1 hh $\rightarrow$ 1 e DQW transition, the PC signal of the aged diode **decreases** to about 65% of the PC signal of the fresh diode. A transition between signal increase and signal decrease upon aging is observed in the narrow energy range between 1.5 and 1.55 eV.

We now compare these results to PC spectra (Fig. 4a) which have been recorded before (*filled circles*) and after (*open circles*) accelerated aging of the Step Index Structure described above. In general, the spectra of the fresh DQW-SIN diode are similar to those of the DQW-GRIN diode. Again, three dominant features, the strong increase at energies above the band edge due to the interband absorption of the 1 hh $\rightarrow$ 1 e DQW transition, the signal increase at energies above 1.8 eV due to the onset of absorption of the $Al_{0.3}Ga_{0.7}As$ layer surrounding the DQW, and the weak defect-related below band gap shoulder are resolved. The effect of aging on the spectra is, however, different for both structures. In the DQW-SIN diode, the below band gap intensity of the PC spectrum increases by as more than a factor of five (Fig. 4b). At energies above 1.55 eV, the PC spectrum changes only slightly, aging leads to a decrease of the DQW absorption related contribution by less than 25%. Similar results have been obtained for a number of DQW-GRIN and DQW-SIN laser diodes under different aging conditions and can be considered typical for the corresponding structures.

2.2 Near-field photocurrent spectra

2.2.1 Image formation in the DQW-GRIN laser diodes. In order to understand the **microscopic** origins of the observed changes in the macroscopic PC spectra and to understand the corresponding aging processes within the laser device, we used a novel technique, namely near-field photocurrent spectroscopy to investigate these diodes. The technique combines the sub-wavelength resolution of near-field optics with tunable laser excitation and allows for selective investigations

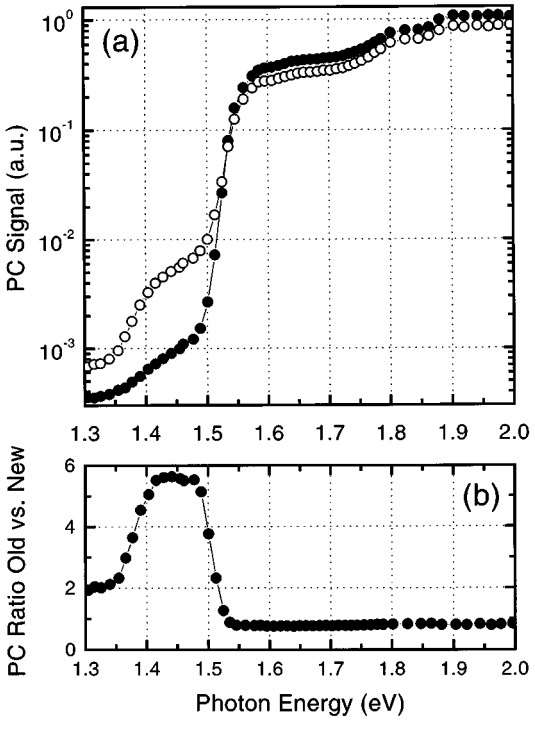

Fig. 4. a Macroscopic room-temperature photocurrent (PC) spectrum (*full circles*, in a.u.) of a fresh step-index high power laser diode array emitting at a photon energy of 1.53 eV before (*full circles*, in a.u.) and after (*open circles*, in a.u.) accelerated aging. Compared to the DQW-GRIN diode array the impurity related below-band gap contribution of the fresh diode is reduced by more than one order of magnitude; **b** Ratio of the macroscopic photocurrent signals after and before accelerated aging of the step-index high power laser diode. The defect or impurity related band at energies between 1.4 and 1.5 eV increases by more than a factor of five upon aging

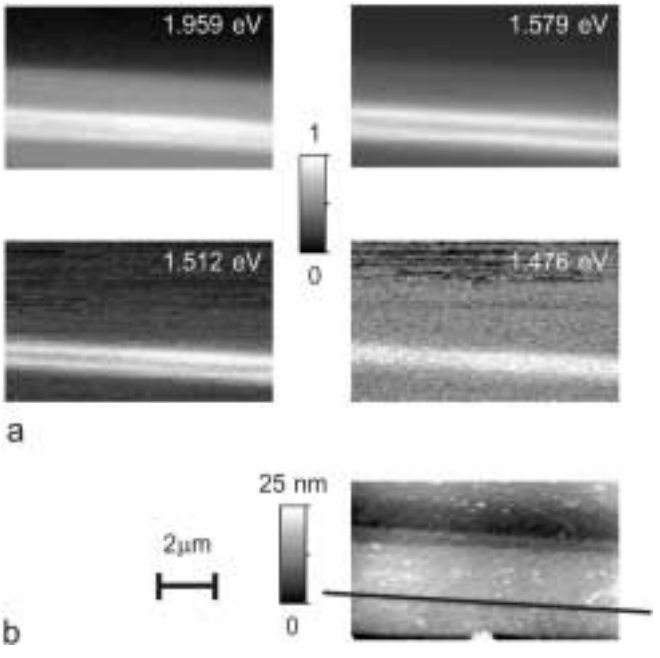

Fig. 5. a Two-dimensional NPC images of a fresh DQW-GRIN laser diode for different excitation energies above (1.959 eV), near (1.579 and 1.512 eV) and below (1.476 eV) the laser photon energy of 1.53 eV. In these images the photoinduced voltage across the p-i-n junction of the laser diode is mapped as a function of the position of the fiber tip. White regions denote regions of high NPC signal while black corresponds to low signal. The scan range in these images is 10 μm × 6 μm and the distance between adjacent data points is 100 nm. Note the pronounced double maximum shape of the NPC signals for excitation energies of 1.579 and 1.512 eV; **b** Shear force image of the topography of the laser diode. The location of the p- and n-doped cladding layers and also the location of the DQW region is resolved in this image. Such images, which are recorded simultaneously with the NPC images, provide a direct spatial correlation between the NPC signal and the layer structure of the laser diode

of specific parts of the laser device. Two-dimensional near-field photocurrent scans for a fresh DQW-GRIN laser diode at four selected excitation energies below and above the band gap are presented in Fig. 5a. These images have been recorded with fiber probes having an aperture diameter of about 200 nm. The presented images are representative examples of a full set of images recorded at about 20 different spectral positions in the range between 1.44 eV and 1.96 eV. The scan area is 10 µm × 6 µm and the separation between adjacent data points 100 nm. In all images, the maximum detected photocurrent has been normalized to unity. In these images, the color white corresponds to a normalized photocurrent of 1, while black corresponds to zero. The images are shown as recorded without filtering or background correction. A simultaneously recorded shear-force topography of the laser facet is shown in Fig. 5b. The location of the DQW layer and the n- and p-doped cladding layers is resolved in these images and permits a direct correlation between NPC image and layer structure of the laser diode. The alignment of the DQW plane, which is slightly tilted against the scan direction of the piezo, is indicated by a solid line. In Fig. 6, cross sections through these images, without normalization, along a line perpendicular to the DQW plane are related to the laser diode structure. Please note that the data for 1.476 eV have been enhanced by a factor of five. Within experimental error, the integrated intensities in these curves follow the macroscopic PC spectrum of Fig. 3a. At an excitation energy of 1.476 eV, i.e. for excitation of the below band gap defect or impurity related band, a narrow NPC signal with a width of 700 nm (full width at half maximum, FWHM) and a maximum in the DQW region is observed. The signal intensity varies only weakly along lines parallel to the DQW plane. At an excitation energy of 1.512 eV, i.e. at the onset of the DQW interband absorption, the signal shape changes drastically into a double maximum structure around the GRIN region and the active region of the laser now appears as a small dip in the center of this structure. The width of this structure is about 1 µm and the two peaks are separated by 450 nm. At 1.579 eV, i.e. for maximum DQW absorption but no GRIN absorption, we observe a similar double maximum structure with a minimum within the active region, but now with a broad background for tip positions within the cladding layers. At 1.959 eV, i.e. for excitation of the DQW and GRIN transitions, this background increases to about 60% of the maximum NPC signal. The double maximum structure becomes slightly broader than at 1.517 eV and the minimum at the DQW is less pronounced.

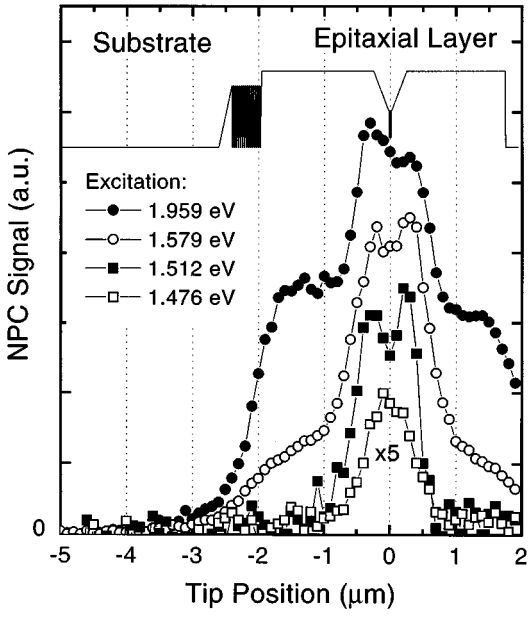

Fig. 6. NPC line scans at excitation energies of 1.959, 1.579, 1.512 and 1.476 eV of the fresh DQW-GRIN laser diode. The scan direction was perpendicular to the active layer. The shape of the conduction band potential is added (*solid line*)

To gain an understanding of the microscopic origins of the strongly excitation energy dependent NPC signals, we analyzed the data by simplified two-dimensional beam propagation calculations. Briefly, the excitation light within the device was modeled as a superposition of evanescent and propagating waves and the layer-specific absorption of each of these waves was considered. We assumed that the electric field distributed which is transmitted through the fiber probe can be modeled by treating the tip as a one-dimensional slit of width d located along the x direction. Within the coordinate system introduced in Fig. 2, the x-axis is perpendicular to the DQW plane, located within the y-z-plane. The y-axis points along the mirror facet of the laser and the z-axis is perpendicular to the mirror facet. The electric field directly behind the tip $E(x,z)$ is then approximated as a sum of plane electromagnetic waves:

$$E(x,z) \propto \int_{-\infty}^{\infty} \frac{\sin(k_x \cdot d/2)}{k_x \cdot d/2} \exp\bigl(\mathrm{i}(k_x \cdot x + k_z \cdot z)\bigr)\,\mathrm{d}k_x\,, \qquad (1)$$

where k_x and k_z denote the components of the wave vector $k_0 = \sqrt{k_x^2 + k_z^2} = 2\pi n_i/\lambda_0$, along the x and z direction, respectively. Here λ_0 denotes the vacuum wavelength of the excitation light and n_i the refractive index of the specific layer of the laser structure.

To further simplify the calculations, we assumed that interference effects are of minor importance for our experiments, and replaced the sum of plane waves by a sum of optical rays which leave the tip under the direction of their wave vector. The relative intensity of each ray is then weighted by the factor $\left(\frac{\sin(k_x \cdot d/2)}{k_x \cdot d/2}\right)^2$. These rays are then propagated through the different layers of the diode structure and the absorption within each of these layers gives rise to photogenerated electron-hole pairs which may then induce the photocurrent signal by getting spatially separated. The laser diode is treated as a p-i-n diode and it is initially assumed that all carriers generated within the undoped GRIN and DQW regions contribute to the photocurrent signal with a yield of unity. Electron-hole pairs generated within the surrounding n- or p-doped cladding layers have to diffuse into the region of the potential gradient and therefore the photocurrent yield p_{PC}, i.e. the probability for these carriers to contribute to the PC signal is taken to decrease exponentially with increasing distance x away from the DQW-GRIN-layers:

$$p_{\mathrm{PC}} = \begin{cases} 1 & \text{if } |x - x_{\mathrm{GRIN}}| \le 0 \\ \exp\bigl(-|x - x_{\mathrm{GRIN}}|/L\bigr) & \text{if } |x - x_{\mathrm{GRIN}}| > 0\,. \end{cases} \qquad (2)$$

Here, x_{GRIN} denotes the location of the graded index–cladding layer boundary, and the ambipolar diffusion length $L$is taken as 0.5 µm.

Depending on the magnitude of the x component of the wave vector k_x, we can distinguish between four different kinds of rays:
(a) $|k_x| > 2\pi n_{\mathrm{DQW}}/\lambda_0$: Fully evanescent rays for which k_z is imaginary within all layers of the diode and for which without absorption, the intensity decays exponentially with increasing z; (b) $2\pi n_{\mathrm{DQW}}/\lambda_0 \geq |k_x| > 2\pi n_{\mathrm{AR}}/\lambda_0$, where n_{AR} is the refractive index of the Al_2O_3 antireflection coating: Rays which are propagating within the AlGaAs layers but evanescent within the Al_2O_3 coating layer, and which consequently are exponentially damped in this layer, (c) $2\pi n_{\mathrm{ref}}/\lambda_0 \geq |k_x| > 2\pi n_{\mathrm{air}}/\lambda_0$: Evanescent rays in air which are transformed into propagating modes in the Al_2O_3 coating layer, and (d) $2\pi n_{\mathrm{air}}/\lambda_0 \geq |k_x|$: Propagating modes in air and the entire laser structure. The simulations now allow us to study the effect of each class of these rays and thus considerably increase the knowledge about the image formation process in near-field photocurrent spectroscopy.

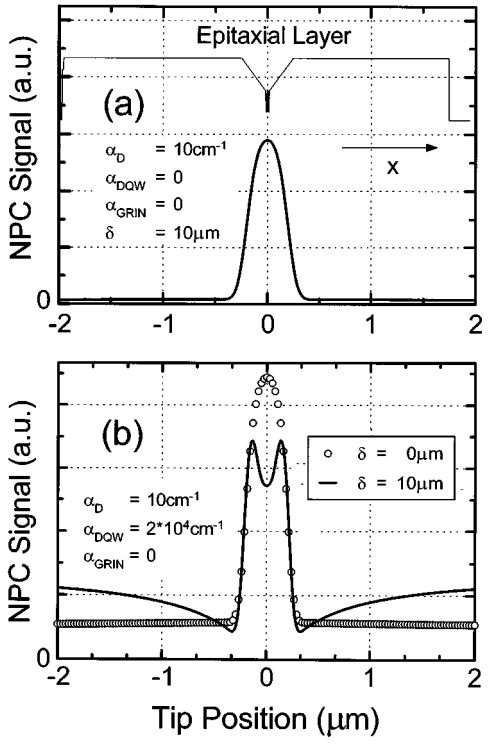

Fig. 7a,b. Results of two-dimensional ray tracing simulations of the near-field photocurrent line scans for the DQW-GRIN laser diode. The fiber probe is modeled as a one-dimensional slit with a width of 200 nm and both propagating and evanescent modes are considered. Details of the model are described in the text. **a** Below band gap excitation: An infrared-active impurity or defect related site with an absorption coefficient $\alpha_{\mathrm{D}} = 10\ \mathrm{cm}^{-1}$ is assumed to be homogeneously distributed within the laser diode. The absorption of both the DQW and the GRIN layers are taken to be negligible. The simulation predicts a narrow peak of the NPC signal inside the DQW region, in agreement with the experimental NPC line scan for $E_{\mathrm{ex}} = 1.494$ eV. The signal arises predominantly from guided propagating modes within the DQW-GRIN wave guide structure; **b** Above band gap excitation: In addition to the defect absorption, an absorption of the active layer with $\alpha_{\mathrm{DQW}} = 2 \times 10^4\ \mathrm{cm}^{-1}$, corresponding roughly to an excitation energy of 1.579 eV is considered. The *open circles* show the result of a simulation neglecting near-surface recombination effects ($\delta = 0\,\mu\mathrm{m}$), which predicts a single-maximum shape of the NPC line scan. This is in contrast to the experiment, e.g. at $E_{\mathrm{ex}} = 1.512$ and also at 1.579 eV. A double maximum shape of the line scans is obtained if the photocurrent yield p_{PC} is assumed to decrease near the mirror facet of the laser diode. The solid line was obtained by taking $p_{\mathrm{PC}} = 1 - \exp(-z/\delta)$, with $\delta = 10\,\mu\mathrm{m}$

At below band gap energies, electron-hole pair generation arises only from defect or impurity related absorption, while neither the DQW, nor the GRIN or doped cladding layers contribute. The impurity distribution is assumed to be homogeneously distributed within the laser structure and the result of a ray tracing calculation for an impurity absorption coefficient of $10\ \mathrm{cm}^{-1}$ is shown in Fig. 7a. The chosen magnitude of the absorption coefficient is reasonable for typical impurity concentrations of about 10^{16}–$10^{17}\ \mathrm{cm}^{-3}$. A variation of the absorption coefficient between 1 and $100\ \mathrm{cm}^{-1}$ changes the signal magnitude but affects the signal shape only weakly. Similar to the experimentally observed NPC line scans at 1.476 eV the simulations show a narrow NPC signal with a single maximum within the DQW region. From the simulations it follows that the NPC signal is dominated by **propagating** waves **guided** inside the GRIN regions. Rays which enter the DQW or GRIN region of the laser diode under a sufficiently small angle α relative to the z-axis, may experience total internal reflection within the graded index region (see Fig. 8). It is important to note that the location along the x-axis at which total internal reflection occurs depends both on the entrance angle α and on the x-position at which the rays enter the DQW/GRIN region. These rays thus propagate only within the intrinsic DQW/GRIN region. The contribution of these guided rays to the NPC signal is very different from that of **unguided** rays for which the entrance angle into the DQW/GRIN region is too large to be internally reflected. These guided waves propagate deep into the DQW/GRIN region so that the effective absorption length is much longer than for unguided waves and they thus create a larger amount of carriers inside the p-i-n region. This waveguiding thus directly explains the high spatial resolution of the NPC signal even though the signal is generated by weakly absorbed propagating modes. Because of the small impurity absorption coefficient and their small penetration depth, evanescent modes are of minor importance for the NPC signal at below band gap energies. The model indicates that their contribution to the signal is at least two orders of magnitude smaller than that of the propagating waves. Due to the strong waveguiding effect, the NPC signals in this diode are also only weakly dependent on minority carrier transport processes.

At excitation energies above 1.5 eV, DQW absorption sets in and the total NPC signal now becomes the sum of a defect related and a DQW related contribution. For small DQW absorption coefficients of less than $10^3\ \mathrm{cm}^{-1}$, the DQW related contribution to NPC signal is again entirely dominated by **propagating** waves **guided** inside the GRIN regions. Within the above model, the shape of the DQW signal is similar to that of the impurity related signal and shows a narrow peak with a single maximum, located inside the DQW region. With increasing DQW absorption coefficient, i.e. with increasing excess energy of the exciting photons, the amplitude of the DQW related NPC signal increases, whereas the shape remains basically unaffected. For large absorption coefficients, the calculations indicate the onset of a much broader background signal for excitation positions within the n- and p-doped cladding layers. This signal arises predominantly from unguided propagating rays which traverse the DQW region only once. For absorption coefficients above $10^3\ \mathrm{cm}^{-1}$, these rays create enough carriers to be detectable in the NPC signal. The amplitude ratio of the contribution from unguided relative to that from guided waves increases with increas-

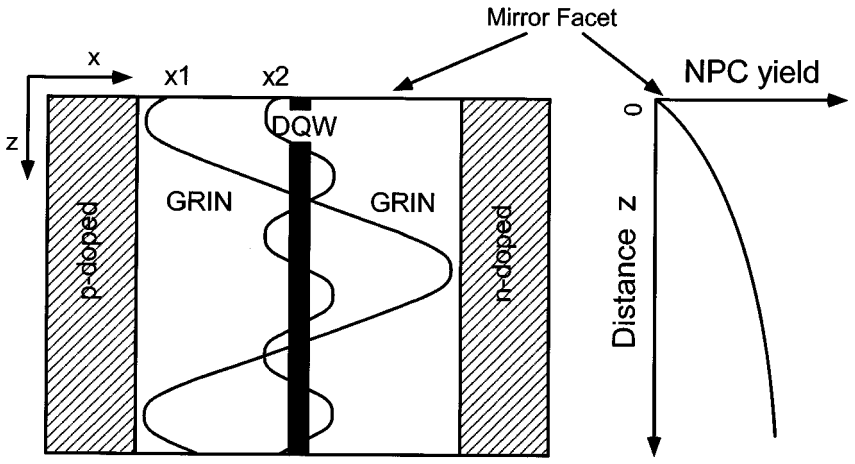

Fig. 8. Effect of nonradiative near-surface recombination in graded-index structures illustrated schematically by considering two guided optical rays emitted at different distances from the active DQW layer. The ray emitted closer to the active layer, at *x*2, experiences a stronger guiding and therefore a stronger absorption within the DQW region. Carriers are generated closer to the mirror facet of the laser than for the ray emitted at *x*1. In the case of strong near-surface recombination, the near-field photocurrent (NPC) yield decreases with decreasing distance *z* to the mirror facet and carriers generated by the ray, starting at *x*2 thus contribute less to the NPC signal than those generated by the ray emitted at *x*1

ing DQW absorption coefficient. This is due to a saturation of the guided wave contribution, since these waves are completely absorbed in the laser diode at high DQW absorption coefficients, while the signal caused by the unguided waves increases roughly linearly with increasing absorption coefficient. This increase of the broad background contribution from unguided waves is confirmed experimentally, compare the NPC line scans for excitation energies of 1.579 eV and 1.512 eV (Fig. 6).

While the growing contribution of background from unguided waves can be consistently explained by our model, the ray tracing simulations predict that the DQW contribution to the NPC line scans should posses a single maximum while the experiments for GRIN structure lasers show a pronounced double maximum shape. The ray tracing simulations showed that this unexpected shape can be attributed to a strong radiationless (near-) surface recombination process. Additional recombination decreases the concentration of excited electron-hole pairs and thus reduces the photocurrent signal [18]. Due to the continuous change of the refractive index within the graded gap region, guided rays that are generated with the tip located close to the DQW region experience a stronger wave guiding than those generated further away from the active region. This is schematically shown in Fig. 8 for two rays emitted from the tip under the same angle but for different tip positions. This difference in waveguiding leads to a variation in penetration depth of the guided waves with tip position. Carrier generation thus occurs closer to the surface if the tip is located closer to the DQW region. These carriers are more strongly affected by recombination processes located at the surface and this results in a smaller NPC signal. Phenomenologically, this idea was incorporated into the ray tracing model by assuming that the photocurrent yield p_{PC}, i.e. the probability with which carriers generated within the DQW/GRIN region contribute to the NPC signal, can be set to zero at the mirror surface ($z = 0$) and increases with increasing distance z as

$$p_{\mathrm{PC}} = 1 - \exp(-z/\delta)\,. \tag{3}$$

Results of ray tracing simulations for a DQW absorption coefficient $\alpha_{\mathrm{DQW}} = 2 \times 10^4\ \mathrm{cm}^{-1}$ and a defect absorption coefficient $\alpha_{\mathrm{D}} = 10\ \mathrm{cm}^{-1}$ including and neglecting near-surface recombination processes are compared in Fig. 7b. In the absence of recombination processes ($\delta = 0\,\mu\mathrm{m}$, *open circles*) a single maximum shape is predicted. The solid line shows the line scan obtained for $\delta = 10\,\mu\mathrm{m}$, while the other parameters remained unchanged. As expected from the qualitative discussion given above, this strong near-surface recombination now leads to a double maximum shape of the NPC line scan, in agreement with the experimental finding. As in the case of below band gap excitation energies, the contribution from waves, which are evanescent within the laser structure or the Al_2O_3 coating are of minor importance.

At excitation energies above 1.8 eV, absorption by the undoped GRIN layers sets in. The corresponding, relatively large absorption coefficient leads to a strong background signal contribution from unguided propagating waves. The signal intensity of this contribution is practically uniform for all tip positions within the doped cladding layers. This is again in agreement with the experiment, as is shown e.g. in Fig. 6 in the line scan for an excitation energy of $E_{\mathrm{ex}} = 1.959$ eV (*solid circles*). Since absorption by the cladding layers is limited to excitation energies above 2.2 eV, their contribution to the NPC signals can be neglected.

2.2.2 Aging of DQW GRIN lasers. We now compare the results which were obtained for a non aged diode to near-field photocurrent spectra for a diode having the same layer structure after performing an accelerated aging procedure. Two points were of particular interest: (1) the effect of aging on the impurity concentration and distribution and (2) its effect on the near-to-surface radiationless recombination process which was resolved in the NPC spectra of the fresh diode. Two-dimensional NPC spectra for energies below, close to and well above the photon energy of the laser for the DQW-GRIN diode before and after accelerated aging are compared in Fig. 9. In addition, Fig. 10 shows one-dimensional NPC scans along a line perpendicular to the active layer of the aged diode. For an excitation energy of $E_{\mathrm{ex}} = 1.959$ eV, both the signal amplitude and the shape of the NPC images are similar before and after aging. The signal consists of a broad plateau for tip positions inside the p- and n-doped cladding layer and a smaller peak inside the DQW-GRIN layer. As mentioned above, the plateau arises from the absorption of unguided propagating waves in the DQW and GRIN layers, while the smaller

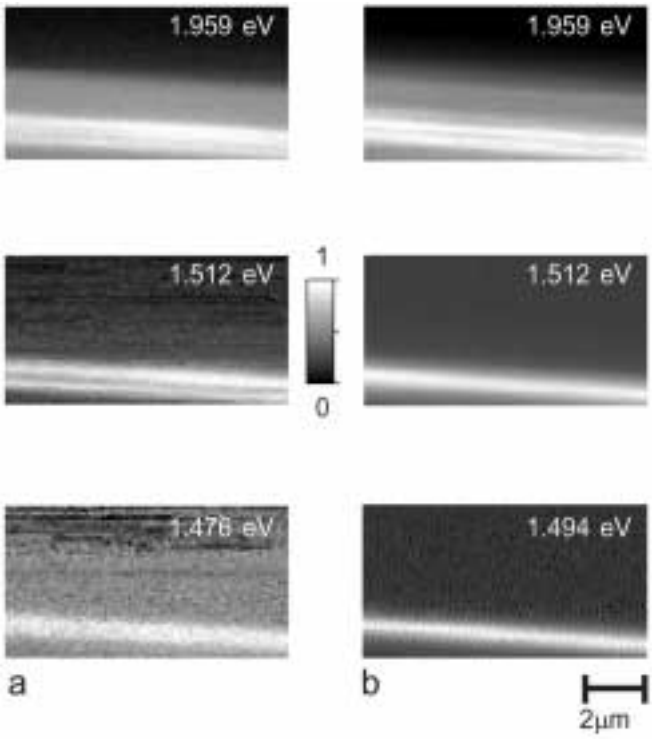

Fig. 9. Two-dimensional NPC images of the DQW-GRIN high power laser diode before (column a) and after (column b) an accelerated aging test. The excitation energy in these experiments was chosen above (1.959 eV), close to (1.512 eV) and below (1.476 eV, respectively 1.492 eV) the band edge of the active layer. While the shapes of the NPC images for excitation energies below and above the band edge change only slightly upon aging, the double maximum structure observed for the fresh diode at $E_{ex} = 1.512$ eV changes into a singly peaked shape for the aged diode

peak is mainly related to the absorption of guided propagating waves within the DQW layer and is only weakly affected by the aging procedure.

The shape of the impurity-related NPC signal at below band gap energies (1.476 eV and 1.494 eV, respectively) changes only slightly upon aging. The line scan for the aged diode fits quite well to a Gaussian line shape with a full width at half maximum of about 600 nm. Compared to the fresh diode, the signal intensity at below band gap energies increases by more than a factor of two upon aging, which is consistent with the aging effect on the macroscopic PC spectrum shown in Fig. 3. This provides evidence for a significant increase of the infrared active defect concentration **within** the DQW-GRIN region upon aging. Moreover - for the first time - the location of the defects is identified.

Aging of the diode has a particularly pronounced effect on the shape of the NPC images for excitation energies near the band gap of the active layer. The NPC signals at excitation energies of 1.512 and 1.531 eV show a single peak located within the DQW region. The width of these peaks increases slightly with increasing excitation energy from 600 nm (FWHM) at 1.476 eV to 700 nm at 1.512 eV and 900 nm at 1.531 eV. These experiments have to be compared to the results for the fresh diode. For this comparison we have chosen an excitation energy of 1.531 eV (Fig. 11). At this excitation energy, the intensity of the macroscopic photocurrent spectrum and thus the integral over the NPC signal along a line perpendicular to the active layer remains unchanged upon aging. Two pronounced changes of the NPC line scan are noticed. First, the double maximum structure observed for tip positions close to the DQW/GRIN region before aging changes into a singly peaked structure after aging. Second, the broad background

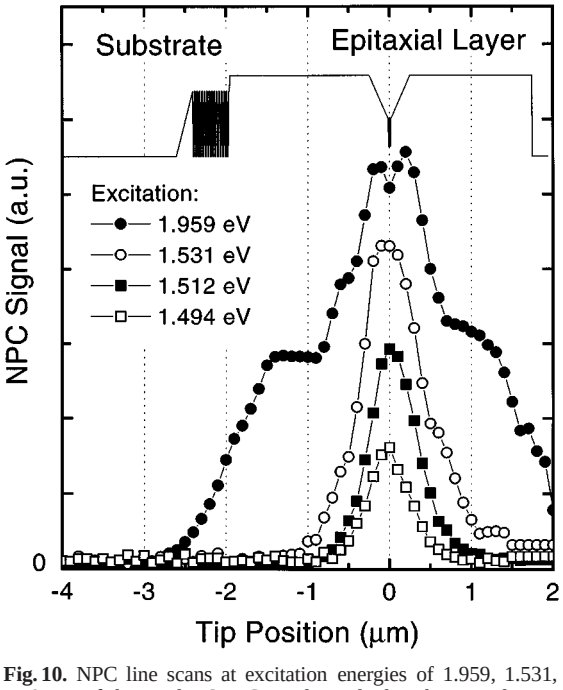

Fig. 10. NPC line scans at excitation energies of 1.959, 1.531, 1.512 and 1.494 eV of the aged DQW-GRIN laser diode. The scan direction was perpendicular to the active layer. The signal maximum for each transient was normalized in order to allow for a better comparison between transients at different excitation energies

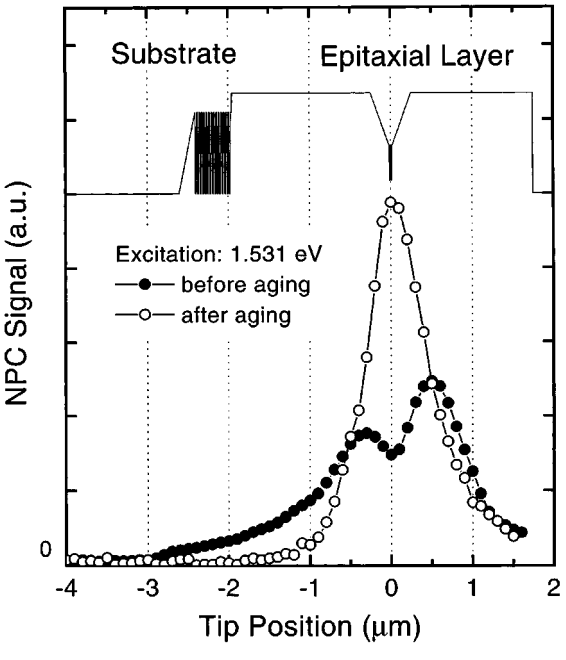

Fig. 11. Comparison of NPC line scans at an excitation energy of 1.531 eV for the DQW-GRIN laser diode before (*closed circles*) and after (*open circles*) accelerated aging. At this excitation energy, the intensity of the macroscopic PC spectrum (Fig. 3), corresponding to the integral over the NPC line scan, remains unchanged. The shape of the conduction band potential is added (*solid line*)

found in the case of the fresh diode for tip positions within the p-doped cladding layer vanishes. This background was shown before to be related to the absorption of unguided waves within the DQW region. **This indicates that the DQW contribution to the NPC signal decreases drastically upon aging**. Since it is highly unlikely that the aging process strongly affects the spectral dependence of the DQW absorption coefficient, we can conclude that this decrease of the DQW related NPC signal arises from a strong increase of (near-) surface recombination processes. Since the overall photocurrent signal does not decrease upon aging, the decrease of the DQW contribution is compensated by an increase of the defect related contribution. While for the fresh diode the broader, double maximum DQW contribution dominates the NPC signal at 1.531 eV the defect related, single maximum contribution becomes dominant upon aging. This directly explains the unexpected change in the NPC signal from a double maximum into a single maximum structure. The increase in the width of the NPC line scan peak of the aged diode with increasing excess energy from 600 nm at 1.476 eV to 900 nm at 1.531 eV indicates that in the aged diode, the DQW contribution to the signal at 1.531 eV does not decrease to zero and is large enough to broaden the total NPC signal.

2.2.3 Step index laser. In this section, the results of the near-field photocurrent experiments obtained for the DQW-GRIN diode array are now compared to experiments on a step index diode array. The layer structure of this array is similar to that of the DQW-GRIN array, expect for the graded gap wave guide layer which is replaced by a 220 nm step index $Al_{0.3}Ga_{0.7}As$ layer with an energy gap of $E_g = 1.8$ eV. These are surrounded by the p- respectively n-doped 1.5–2 µm thick $Al_{0.6}Ga_{0.4}As$ cladding layers with an energy gap (E_g) of about 2.2 eV. As for the DQW-GRIN structure, the laser emission is at 1.53 eV.

Waveguiding in this step index structure differs significantly from that in the graded index structure since the refractive index of the 220 nm step index layer is constant and total internal reflection can thus only occur at the boundary between the step index and the surrounding $Al_{0.6}Ga_{0.4}As$ cladding layers. The main emphasis of these experiments is to investigate the effect of this difference in wave guiding on the near-field photocurrent image formation. In particular, it was of interest to check the validity of the ray-tracing approach and to check the conclusions which were drawn on the effect of radiationless near-surface recombination process on the near-field images. In fresh step index arrays, the defect related contribution to the photocurrent is more than an order of magnitude smaller than in the case of the DQW-GRIN diode, which simplifies a separation between defect related and DQW related contributions (see Fig. 4).

Two-dimensional NPC images at different excitation energies for a step index diode before and after accelerated aging are shown in Fig. 12. The scan area in these images is 10 µm × 6 µm and the separation between adjacent data points 100 nm. The maximum intensity of each image has again been normalized to unity. Scans along a line perpendicular to the active layer are depicted in Fig. 13 for the fresh diode array and in Fig. 14 after performing the accelerated aging procedure. We note that in these images, the maximum of each line scan was rescaled in order to allow for a better comparison between transients at different excitation energies. Within

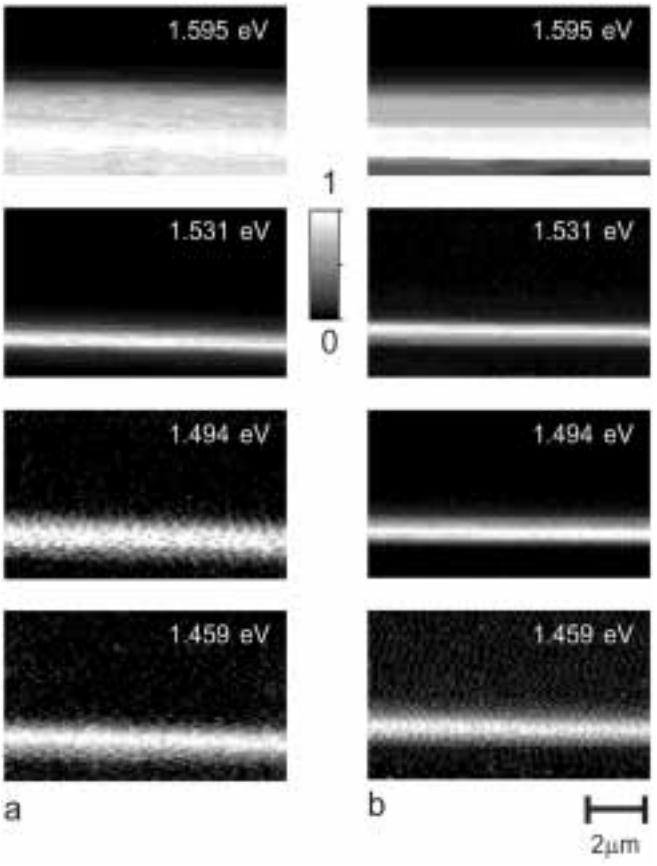

Fig. 12. Two-dimensional NPC images of a step index laser diode for different excitation energies above (1.959 eV), near (1.531 eV) and below (1.494 and 1.459 eV) the laser emission energy of 1.53 eV before and after accelerated aging of the laser diode. The scan range in these images is 10 µm × 6 µm and the distance between adjacent data points is 100 nm

experimental error, the spectral dependence of the signal amplitude of the NPC images follows closely the macroscopic PC spectrum and varies by about three orders of magnitude over the range of excitation energies.

The results obtained for an excitation energy of 1.959 eV, i.e. for excitation well above the band edge of the active layer are similar to those obtained for the DQW-GRIN structure. The signal consists again of a broad plateau for tip positions inside the p- and n-doped cladding layer and a smaller peak located within the step index wave guide layer. The plateau can be attributed to absorption of unguided propagating waves within the DQW and SIN layers, while the smaller peak is mainly related to the absorption of guided propagating waves within the DQW layer. As for the DQW-GRIN structure, the NPC image is only weakly affected by the aging procedure for this above bandgap wavelength.

Also the shapes of the NPC images for excitation energies below the band gap of the active layer, i.e. at $E_{ex} = 1.459$ eV and $E_{ex} = 1.494$ eV, are only weakly affected by the aging procedure. As for the DQW-GRIN array, a narrow structure with a single peak inside the center of the wave guide structure is found. This signal can again be assigned to an infrared active defect- or impurity related contribution. The width of the signal varies between 600 and 700 nm and does not change significantly upon aging. The signal shape can be reproduced qualitatively within the ray tracing model introduced above,

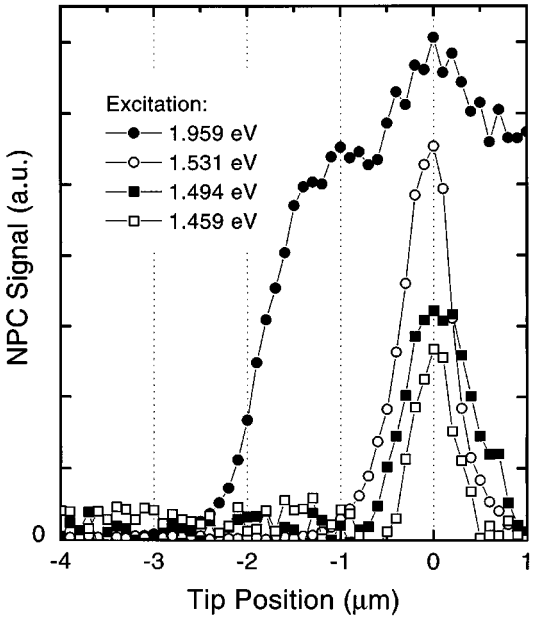

Fig. 13. NPC line scans at excitation energies of 1.959, 1.531, 1.494 and 1.459 eV of the fresh step index laser diode. The scan direction was perpendicular to the active layer, located at a tip position of 0 μm. The ratio of the NPC intensity at different excitation energies follows closely the macroscopic PC spectrum shown in Fig. 4

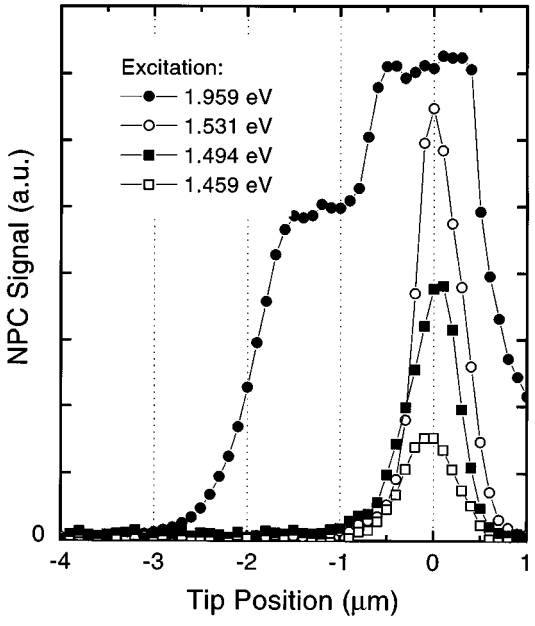

Fig. 14. NPC line scans at excitation energies of 1.959, 1.531, 1.494 and 1.459 eV of the step index laser diode after accelerated aging. The scan direction was perpendicular to the active layer, located at a tip position of 0 μm

if a small defect related absorption coefficient on the order of 1 cm^{-1} is assumed to be homogeneously distributed within the laser device. Here, the NPC signal is entirely due to the absorption of propagating waves guided within the step index structure and the signal shape is due to waveguiding effects while minority carrier transport is of minor importance. The role of evanescent modes is negligible. In this diode, aging of the laser diode leads to a strong increase of the defect concentration and therefore to an increase of the NPC signal magnitude by more than a factor of five. Because of the dominance of waveguiding effects, the shape of the NPC signal is only weakly affected by the change of the defect concentration, in agreement with simulations.

The NPC signal intensity of the fresh diode increases by about a factor of 20 as the excitation energy is increased from 1.494 eV to 1.531 eV. This is due to the onset of DQW absorption, which dominates the NPC signal at $E_{ex} = 1.531$ eV. Unlike for the DQW-GRIN diode, the shape of the NPC signal does **not** change drastically at the onset of DQW absorption. The NPC signal still shows a **single** maximum shape with its peak located at the center of the wave guide structure. For both the fresh and the aged diode, the width of the NPC signal is about 600 to 650 nm and, as for the GRIN structure, the signal amplitude is approximately the same in both experiments. This singly peaked shape has to be compared to the pronounced double maximum feature of the fresh GRIN structure. Within the ray tracing model introduced above, this change in the signal from a double maximum into a single maximum shape upon changing of the wave guide layer from a graded index into step index structure is readily explained. Consider again two guided rays emitted from a point light source located within the step index layer. As in Fig. 7, the rays are assumed to be emitted under the same angle but for different tip positions relative to the active layer. Since the refractive index profile is constant within the step index, both rays are now totally reflected at the boundary between the step index and the surrounding cladding layer. Therefore, for the step index structure, both rays experience the same guiding and consequently also the same absorption by the active DQW layer. Unlike for the graded index structure, the penetration depth of the rays is **not** dependent on the tip position. Even in the case of strong near-surface recombination processes, the photocurrent yield does not depend on the tip location and this explains why the shape of the NPC signals does not change at the onset of strong DQW absorption.

We can conclude, that the introduced ray tracing model allows to qualitatively explain the NPC signals for both the graded index and the step index structures, and that indeed the wave guiding characteristics of the diode layers have a particularly strong influence on the NPC image formation process. This provides additional evidence for the importance of propagating guided beams for the NPC signals. In step index structures, due to the insensitivity of the wave guide properties to the exact location of the excitation source within the wave guide layer, (near-) surface recombination effects have only a minor effect on the shape of the NPC images.

3 Summary and conclusion

In this paper, the first comparative study of spatially resolved near-field photocurrent spectra for two high power laser diode arrays with different wave guide characteristics was presented before and after accelerated aging of the laser device. In these experiments sub-wavelength spatial resolution was demonstrated by exciting the laser device through a nanometer sized aperture located at the of a near-field fiber probe. Tuning of the excitation energy across the band gap energy of the laser allowed us to study specific components of the laser device experiments. At below band gap energies car-

rier generation is dominated by absorption of an infrared active defect- or impurity related site, while at energies above the laser emission at 1.53 eV absorption of the active double quantum well layer dominates. In the DQW-GRIN diode array, a strong variation of the shape of the NPC images with excitation energy was observed. In particular, the DQW related NPC signal showed a pronounced double maximum structure. With the help of a ray tracing model, the NPC image contrast was found to arise predominantly from propagating waves guided within the graded gap layer and the observed double maximum was assigned to arise from (near-) surface radiationless recombination effects. The line shape of the near-field scans was shown to depend strongly on the magnitude of the surface recombination velocity so that near-field photocurrent spectroscopy presents a powerful tool for the microscopic analysis of aging effects on surface recombination processes. A quantitative extraction of surface recombination velocities requires however a more detailed analysis of the experimental data in the light of refined microscopic models [19]. Such an analysis is currently underway. NPC experiments performed after accelerated aging of the DQW-GRIN structure presented direct evidence for the strong aging-induced increase of the defect concentration within the wave guide layer of the device. Concomitantly, the DQW contribution to the NPC signal decreased which is an indication for the increase of surface recombination velocities upon aging. Here, it will be of particular interest to see whether the increase of surface recombination effects is directly related to the growth of the infrared active defect concentration and how these effects vary among different emitters of the laser array.

The conclusions drawn from the study of the DQW-GRIN structure were strongly supported by a comparative study of a diode laser array of a similar composition, except for a different, step index, wave guide structure. The change in wave guide structure makes the shape of the NPC images less sensitive to surface recombination processes so that in this structure the aging procedure mainly affects the magnitude of the NPC signals.

So far our discussion did not clarify the nature of the defect accompanied to the aging. We pointed out that native infrared active defects contribute to the below-band gap PC signal. These defects are known to be readily observable in DLTS spectra [20] and such measurements are currently underway. We note however, that due to the dominance of waveguiding effects on the NPC image formation process, the current experiments can also be explained by the migration of impurity related defects into the wave guide layer. This will be the subject of further investigations.

In summary, we demonstrated that near-field photocurrent spectroscopy has the potential to provide direct insight into the microscopic processes of aging-induced defect creation and surface recombination in the active region of high-power laser diodes.

Acknowledgements. The authors would like to thank A. Bärwolff and U. Menzel for helpful discussions, Ch. Lier for expert technical assistance and G. Behme for help in preparing some of the figures. Special thanks are due to F.X. Daiminger from JENOPTIK LASERDIODE GMBH and J. Luft from Siemens AG for providing us with the high quality laser diode samples. In particular, we wish to thank T. Elsaesser for careful reading of the manuscript and continuous support of this work.

References

1. M. Fukuda: *Reliability and Degradation of Semiconductor Lasers and LEDs* (Artech House, Boston 1991)
2. P. G. Eliseev: *Reliability Problems of Semiconductor Lasers* (Nova Science, Commack 1991)
3. A. Richter, J.W. Tomm, Ch. Lienau, J. Luft: Appl. Phys. Lett. **69**, 3981 (1996)
4. S.K. Buratto, J.W.P. Hsu, E. Betzig, J.K. Trautman, R.B. Bylsma, C.C. Bahr, and M.J. Cardillo: Appl. Phys. Lett. **65**, 2654 (1994)
5. M.S. Ünlü, B.B. Goldberg, W.D. Herzog, D. Sun, and E. Towe: Appl. Phys. Lett. **67**, 1862 (1995)
6. B.B. Goldberg, M.S. Ünlü, W.D. Herzog, H.F. Ghaemi, and E. Towe: IEEE J. Selected Topics Quant. El. **1**, 1073 (1995)
7. E. Betzig, J.K. Trautman, T.D. Harris, J.S. Weiner, and R.L. Kostelak: Science **251**, 1468 (1991)
8. E. Betzig, P.L. Finn, and J.S. Weiner: Appl. Phys. Lett **60**, 2484 (1992)
9. P.C. Yang, Y. Chen, M. Vaez-Irvani: J. Appl. Phys. **71**, 2499 (1992)
10. Ch. Lienau, A. Richter, and Th. Elsaesser: Appl. Phys. Lett. **69**, 325 (1996)
11. J.W. Tomm, A. Bärwolff, U. Menzel, M. Vo, R. Puchert, Th. Elsaesser, F.X. Daiminger, S. Heinemann, and J. Luft: J. Appl. Phys. **81**, 2059 (1997)
12. M. Voss, C. Lier, U. Menzel, A. Bärwolff, and T. Elsaesser: J. Appl. Phys. **79**, 1170 (1996)
13. J.W. Tomm, A. Bärwolff, A. Gerhard, and J. Donnecker: Proc. 47th Electronic Components and Technology Conference, accepted for publication
14. G.M. Martin: Appl. Phys. Lett. **39**, 747 (1981)
15. S. Tüzemen, and M.R. Brozel, Appl. Surf. Science **50**, 395 (1991)
16. K. Saarinen, S. Kuisma, P. Hautojärvi, C. Corbel, and C. LeBerre: Phys. Rev. Lett. **70**, 2794 (1993)
17. M. Lannoo: *Handbook of Semiconductors*, Vol. 2, ed. by T.S. Moss (Elsevier, Amsterdam 1994)
18. H.J. Leamy: J. Appl. Phys. **53**, R51 (1982)
19. K.L. Luke: J. Appl. Phys. **75**, 1523 (1994)
20. J. Lagowski, D.G. Lin, T.P. Chen, M. Skowronski, and H.C. Gatos: Appl. Phys. Lett. **47**, 929 (1985)